RSC Advances

PAPER

View Article Online
View Journal | View Issue

Cite this: *RSC Adv.*, 2020, **10**, 13394

One-step dry synthesis of an iron based nano-biocomposite for controlled release of drugs†

Sophia Varghese, Jai Prakash Chaudhary and Chinmay Ghoroi *

Received 5th February 2020
Accepted 23rd March 2020

DOI: 10.1039/d0ra01133a

rsc.li/rsc-advances

Bio-based drug carriers have gained significant importance in Control Drug Delivery Systems (CDDS). In the present work, a new iron-based magnetic nano bio-composite (nano-Fe-CNB) is developed in a one-step dry calcination process (solventless) using a seaweed-based biopolymer. The detailed analysis of the developed nano Fe-CNB is carried out using FE-SEM, HR-TEM, P-XRD, XPS, Raman spectroscopy, FTIR *etc.* and shows that nano-Fe-CNB consists of nanoparticles of 5–10 nm decorated on 7–8 nm thick 2-D graphitic carbon material. The impregnation of nano-Fe-CNB into the calcium alginate (CA) hydrogel beads is found to have good drug loading capacity as well as pH responsive control release behavior which is demonstrated using doxorubicin (DOX) as a model cancer drug. The drug loading experiments exhibit ~94% loading of DOX and release shows ~38% and ~8% release of DOX at pH 5.4 and 7.4 respectively. The developed nano Fe-CNB facilitates strong electrostatic interactions with cationic DOX molecules at pH 7.4 and thereby restricts the release of the drug at physiological pH. However, at cancer cell pH (5.4), the interaction between the drug and nano-Fe-CNB reduces which facilitates more drug release at pH 5.4. Thus, the developed nano-biocomposite has the potential to reduce the undesired side effects associated with faster release of drugs.

Introduction

Recent statistics by the World Health Organization demonstrate that the majority of deaths are caused due to cancer and have estimated approximately 9.6 million deaths in 2018.[1,2] The major route of administration for chemotherapy treatment is through intravenous injections, which use anticancer agents responsible for burst release effect and destroy normal cells along with tumor cells.[2–4] For example, doxorubicin (DOX),[5] an anticancer drug, is a commonly used model drug (commercially available as Adriamycin) with solubility 50 mg ml^{-1} used to treat various solid tumors of the breast, ovary, *etc.* However, DOX has several side effects due to burst release such as nausea, diarrhea, anemia, and decreased appetite. Hence, studies are carried out for the controlled release of DOX. Thus, the controlled release (CR) of anticancer drugs is preferred for targeting the drug to the local tumor site, which helps to attain the therapeutic concentrations and reduces the damage to the normal tissues and cells.[3,6,7] In addition, it reduces the frequency of drug intake and side effects. However, the release profile of these drugs is strongly influenced by the choice of carriers.[2,6]

Bio-polymers are of great interest in the field of Control Drug Delivery Systems (CDDS) because of its advantages such as bio-compatibility, low toxicity, and ease of availability. Sodium alginate, a bio-polymer derived from brown algae possesses the unique feature of gel formation in the acidic and basic medium and also has additional benefits such as bio-compatibility, biodegradability and low toxicity.[6,8,9] Moreover, the incorporation of inorganic and organic nanoparticles in hydrogels prepared from bio-polymer enhances the drug loading and controlled release behavior. These nano-materials include silica,[10] gold,[2,11–13] Fe_3O_4,[4,14–16] carbon nanotubes (CNT),[17–19] including 2-D material like graphene oxide (GO)[4,20] *etc.* There are several controlled release studies reported for DOX in the literature[1,2,4,7,11,14,17] using GO,[4,20] carbon dots, CNT and super-magnetic nanoparticles such as Fe_3O_4.[4,13–15,21] The release of DOX from GO, CNT and carbon dots are preferred due to its higher drug loading capacity (77–90%), and the larger surface area available in the layered materials.[17,18] Xue *et al.* studied the subcellular delivery of doxorubicin from pH-responsive alginate nanogel.[6] The sustainable release of DOX at 5.0 pH is reported to be >90%, and at 7.4 pH, the corresponding release is 38% in 40 h.[6] However, the drug release at physiological pH (7.4) is much higher. Suarasan *et al.* studied the controlled release of DOX, which is incorporated in the nanotherapeutic delivery system consisting of gelatin-coated gold nanoparticles.[2] The amount of DOX released at 4.6 pH and 7.4 pH after 24 h are

DryProTech Lab., Chemical Engineering, Indian Institute of Technology Gandhinagar, Palaj, Gandhinagar-382355, Gujarat, India. E-mail: chinmayg@iitgn.ac.in; Tel: +91-79-23952405

† Electronic supplementary information (ESI) available: Thermal and magnetic behavior; schematics for loading of DOX on Fe-CNB CA; fluorescence microscopy images of HeLa cells subjected to treatment for 3, 8 and 24 h. See DOI: 10.1039/d0ra01133a

approximately 80% and 25%, respectively.[2] But, the release of DOX in physiological pH is relatively high at 24 h. Deng *et al.* designed a hybrid microcapsule (h-MC) using sodium alginate, chitosan, hyaluronic acid along with iron oxide and graphene oxide by a layer-by-layer technique to study the *in vivo* antitumor therapy using DOX. The results exhibited that the DOX was released more from h-MC at acidic pH 5.4 as compared to 7.4 pH indicating pH-responsive behavior of h-MC composite.[4] Similarly, Cao *et al.* carried out the targeted delivery of DOX from modified multi-walled carbon nanotubes using hyaluronic acid.[17] The *in vitro* studies demonstrated that DOX release is ~54% at 5.4 pH and about 40% at physiological pH 7.4 in 48 h.[17] However, the release of 40% at physiological pH is considerably high. The literature shows that the most of the release studies using different nano-carriers are conducted at tumor cells pH (5.4) and physiological pH (7.4).[2,6,17] Though desired controlled release is reported for several cases at 5.4 pH, the drug release at physiological pH is quite high (in the range of ~25–54%) which is highly undesirable.

The present study focuses on developing a new magnetic nano-biocomposite (nano Fe-CNB) using the facile route of synthesis, which is pH responsive and its application thereof in the controlled release of the drug (DOX as a model drug) known as a red devil. In the first part (material development), the material is developed using a one-step dry calcination process without the usage of any solvent. The nano Fe-CNB is explored in detail using various characterization techniques to understand the material property. The developed nano Fe-CNB exhibits pH and magnetic responsive behavior. The nano Fe-CNB consist of 2-D layered carbon material decorated with magnetic Fe based core in a single step, without any solvent or post-processing. In the second part (application), the nano Fe-CNB is used to study the controlled release of the anticancer drug DOX. The developed nano Fe-CNB is further embedded into the bio-polymeric matrix to form the Smart Drug Delivery System (SDDS) for the controlled release of DOX. The magnetic nano bio-composite exhibits pH responsive behavior due to Fe-based core coupled with layered carbon material. After DOX loading on nano Fe-CNB CA beads, the release studies were performed at 5.4 and 7.4 mimicking the pH of tumor cells and physiological along with controlled experiments using DOX-loaded CA beads (without the addition of nano Fe-CNB). The DOX-loaded Fe-CNB CA shows high drug loading capacity and can maintain a very low concentration of the drug in physiological pH. The developed new SDDS is capable of very minimal release in physiological pH (7.4) which is desirable and with improved efficacy to release the drug at tumor cells pH (5.4).

Materials and methods

Materials

The alginic acid sodium salt from (Fluka Biochemika) was purchased, iron ammonium sulphate (MERCK, Extra Pure), calcium chloride·$2H_2O$ (Extra Pure, MERCK), doxorubicin hydrochloride (TCI, chemicals), were used as received. Acetic buffer solutions (5.4 pH) and phosphate buffer solution (PBS) (7.4 pH) for drug release studies were used. The dialysis tube (Sigma Aldrich, 10 kDa) was used.

Preparation of nano biocomposite (nano Fe-CNB) and nano Fe-CNB impregnated calcium alginate matrix (nano Fe-CNB CA)

Nano Fe-CNB was prepared using sodium alginate and iron ammonium sulphate salt. Initially, sodium alginate was mixed with iron ammonium sulphate to prepare homogeneous slurry and was oven-dried. The oven-dried sample was then subjected to calcination under N_2 atmosphere for 3 h at 800 °C with a ramp rate of 5 °C to obtain Fe-based nano-biocomposite (nano Fe-CNB).

The nano Fe-CNB (0.048 wt%) was added into the sodium alginate solution (1.5 wt%) under continuous stirring conditions. The selection of nano Fe-CNB was based on the higher drug loading at the particular weight percent of nano biocomposite. Sodium alginate solution containing nano Fe-CNB was added dropwise with pipette in calcium chloride solution (0.5 wt% prepared) to obtain the nano-Fe-CNB impregnated calcium alginate bead (nano Fe-CNB CA). The experimental steps are represented in Fig. 1. The developed nano Fe-CNB-CA were kept in $CaCl_2$ solution for 6 h to ensure complete gelation and further rinsed with Milli Q water (resistivity ~ 18 MΩ) for removal of excess chloride present. Then the hydrogels were subjected to lyophilization before used for drug loading.

Drug loading on calcium alginate (CA) and nano Fe-CNB impregnated calcium alginate (nano Fe-CNB CA) and the release study

The drug (DOX) loading and release studies from the CA and nano Fe-CNB CA were determined by using the absorbance value from Biotech Cytation 5 Imaging reader (USA) in 96 well plates. The standard drug solution of DOX was prepared in Milli Q water (0.2 mg ml^{-1}). The lyophilized CA and nano Fe-CNB CA beads were subjected to the standard DOX solution (0.2 mg ml^{-1}) for 24 h to load the drug. The drug (DOX) solution was decanted after 24 h to separate the CA and nano Fe-CNB CA. The DOX loaded CA and nano Fe-CNB CA beads were further lyophilized. The decanted solution was then subjected to UV-analysis to determine the percentage of drug remaining in the solution. The UV at (λ = 480 nm) spectra for standard DOX solution (C_i) and that of remaining drug solution after loading (C_f) was then used to calculate the drug uptake by the CA and Fe-CNB CA matrix respectively. The amount of drug uptake by the matrix was quantified using eqn (1). All the loading experiments were performed in triplicates, and the mean value with standard deviation (SD) for the same was reported. A similar method of drug loading for hydrogels was reported elsewhere.[22]

$$\text{Drug loading efficiency (\%)} = (C_i - C_f/C_i) \times 100 \quad (1)$$

The DOX release studies were carried out at 37 °C and 100 rpm rotation at different pH 5.4 (acetic buffer) and 7.4 (phosphate buffer) solution (25 ml). The DOX-loaded Fe-CNB CA was taken in a dialysis tube (pre-activated) along with 3 ml

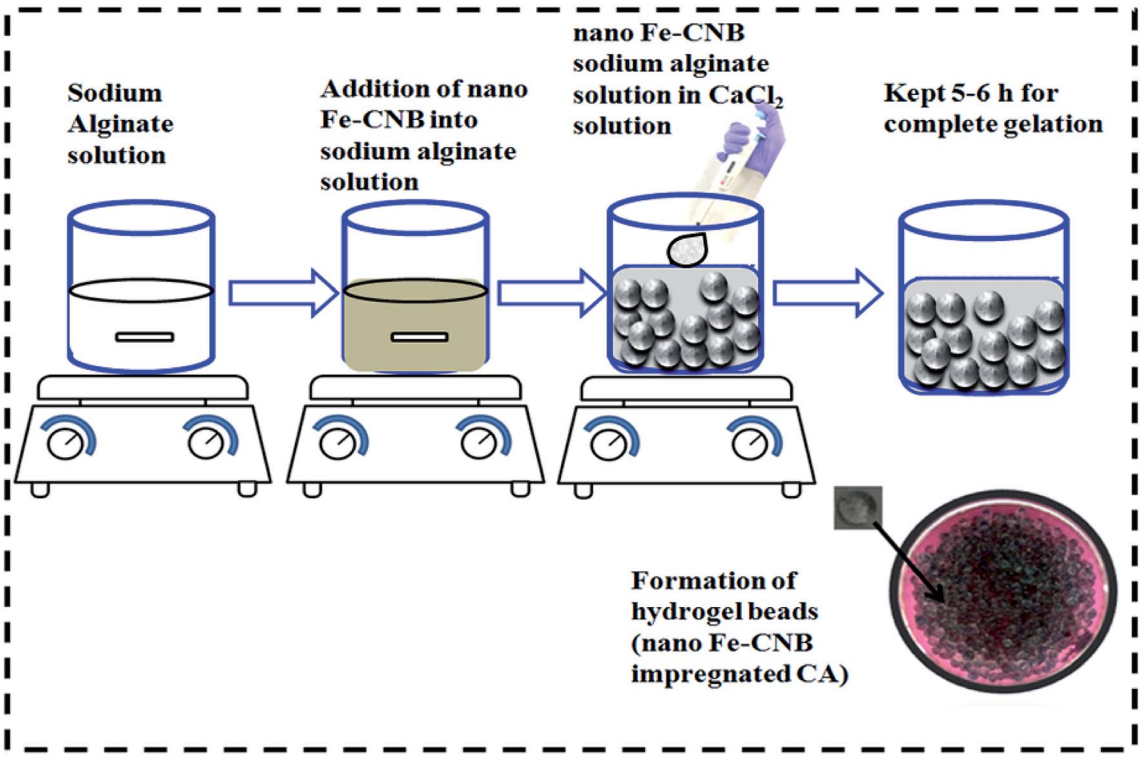

Fig. 1 Schematic illustration of the preparation of nano Fe-CNB embedded calcium alginate (CA) hydrogel beads.

of the respective buffer solution. The dialysis tube was immersed in the beakers containing buffers (25 ml) of pH 5.4 and pH 7.4 at 37 °C respectively. At different time intervals, 400 μl of the sample was withdrawn and replaced by fresh buffer solutions every time. The percent release of DOX was measured by UV-visible spectrophotometer at 480 nm. Similar studies were performed for DOX-CA (control). The release was performed in triplicates, and the mean value with SD of the same was reported. The statistical analysis of the release profile was performed using two way ANOVA test using Graph pad prism software version 5.0. The drug release was quantified using eqn (2).

The following equation determined the drug release

$$\text{Drug release } (\%) = \frac{I}{I_0} \times 100 \qquad (2)$$

where I = emission intensity of released DOX, I_0 = initial emission of total intensity DOX-loaded on to nano Fe-CNB CA.

Characterizations

The morphological changes were investigated by Field Emission Scanning Electron Microscopy (FE-SEM) (JEOL, USA) operated at 5.0 kV and a working distance of 8–10 mm. High-Resolution Transmission Electron Microscopy (HR-TEM) was used to depict the morphology and size, which was recorded using HR-TEM (JEOL JEM 2100) operated at a voltage of 200 kV. Material characterizations, as well as drug–carrier interactions, were evidenced by the Fourier Transform Infrared Spectroscopy (FTIR) (PerkinElmer, IR spectra) ATR method from wavenumber (4000 cm^{-1} to 400 cm^{-1}) and X-ray Photoelectron Spectra (XPS) of ULVA-PHI INC (Japan) with AES module with Ar ion (PHI 5000 Versa probe II) was used. The thermal stability of the prepared nano Fe-CNB is determined using Thermal Gravimetric Analysis (TGA) at temperature 25–850 °C at the heating rate 10 K min^{-1} using (NETZSCH, STA 449 F3 Jupiter). The changes in the crystalline nature and the crystal properties were studied using Powder X-ray Diffraction (P-XRD) (Bruker, D8 Discover) at 40 kV, 30 mA from 2θ values (5–90) at the step size 0.02 with scan speed 0.2. The porous nature and the surface area measurements were performed to determine the surface area and pore volume distribution using the BET surface area analyzer (Micromeritics, U.S.A.). The degassing was performed in a nitrogen environment at 120 °C for 10 h. The determination of carbon material and the presence of Fe(O) was carried out using Raman Spectroscopy (NXR FT-Raman, U.S.A.) from wavenumber (200 cm^{-1} to 4000 cm^{-1}). The magnetic property of the nano Fe-CNB was determined using an external magnet and Vibrating Sample Magnetometer (VSM) (PAR 155) by varying the magnetic field (tesla) from −3.0 T to +3.0 T at room temperature (297 K). The drug loading and release studies were carried out in Biotech Cytation 5 Imaging reader (USA) plate reader equipped with 96 well plates.

Results and discussion

Size and surface morphology

The HR-TEM experiments show the morphology and the size of the developed nano Fe-CNB material. Fig. 2A depicts the high-resolution TEM images showing clusters of carbon layer with

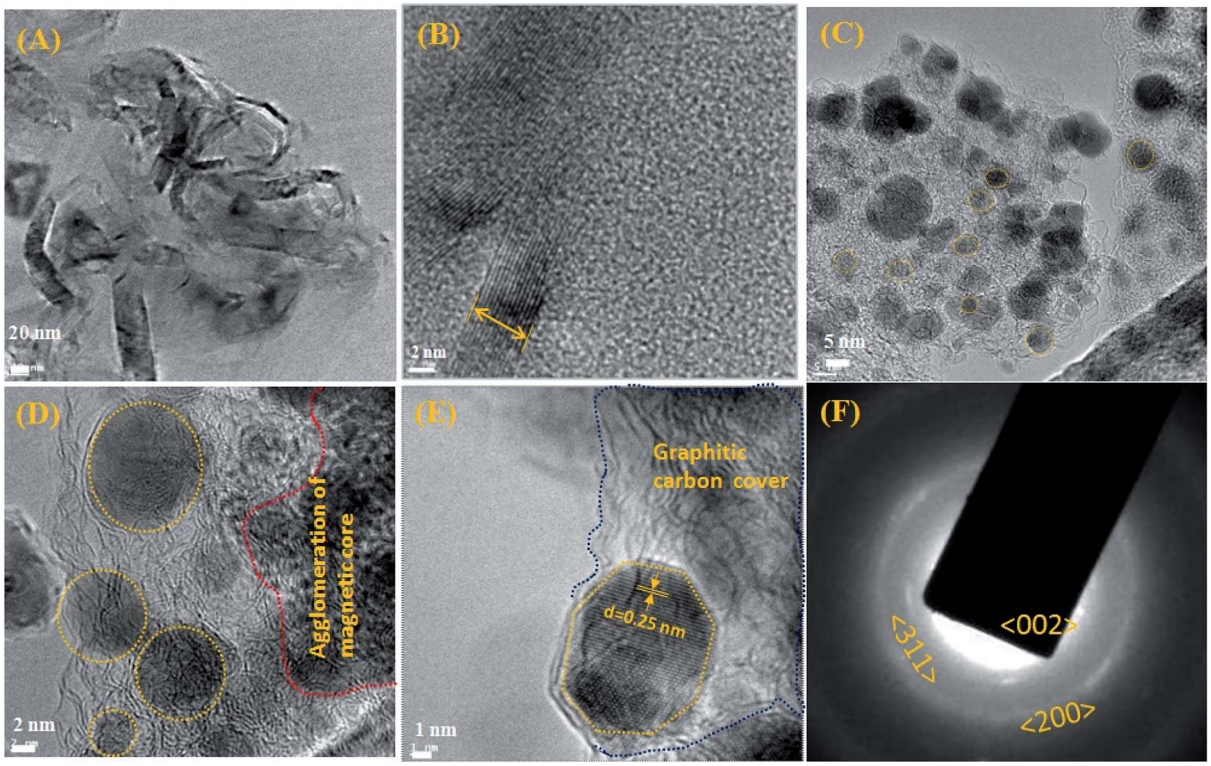

Fig. 2 Exhibits the HR-TEM of nano Fe-CNB, (A) depicts the high-resolution TEM images showing clusters of carbon layer with embedded nanoparticles, (B) exhibits the thickness of the graphitic carbon sheet of 7–8 nm. (C) and (D) shows graphitic carbon having randomly scattered Fe-CNB magnetic core (highlighted using yellow dashed lines) of size 5–10 nm at different magnifications. (E) Lattice fringes of magnetic core (highlighted using yellow dotted line) with *d* spacing of 0.25 nm embedded in the layered graphitic carbon (highlighted using blue dotted line). (F) depicts the SAED pattern of Fe-CNB.

embedded nanoparticles. Fig. 2B exhibits the thickness of the graphitic carbon sheet of 7–8 nm. Fig. 2C and D shows the graphitic carbon having randomly scattered Fe-based magnetic core (highlighted using yellow dashed lines) of size 5–10 nm at different magnifications. Also, there exists agglomeration at few places of magnetic cores as exhibited in Fig. 2D. The lattice fringes of the magnetic core with a *d* spacing of 0.25 nm are embedded in the layered graphitic carbon which is shown in Fig. 2E. The Fig. 2F depicts the SAED pattern of nano Fe-CNB which helps to confirm the presence of Fe, Fe_3O_4, and graphitic carbon from the lattice planes (200), (311) and (002) respectively. The diffused pattern of the ring observed indicates the presence of carbon in the material. The HR-TEM results confirm that nano bio-composite consists of carbon based layered material with embedded Fe magnetic cores. The single-step calcination process is capable of hosting the Fe-based magnetic core on layered carbon material without the usage of the solvent and post-processing step as in conventional method. Thus, the developed nano Fe-CNB is further explored with different techniques.

The morphological changes of a cross-section of calcium alginate beads are demonstrated in Fig. 3A, which exhibits the flake-like structure with a smooth surface. While Fig. 3B demonstrates the FE-SEM for a cross-section of a cut piece of calcium alginate bead, which resembles the blooming of the flower bud. Fig. 3C represents the nano Fe-CNB material showing highly porous nature. Fig. 3D represents the cross-sectional view of nano-Fe-CNB CA beads, which indicates the presence of thin layered material on to the surface of the flakes. Fig. 3E represents the cross-section for DOX-loaded Fe-CNB CA, where the presence of the small particles on to the surface of Fe-CNB CA is observed. At the higher magnification, it is identical to the spherical shape of DOX and is found to be in good agreement with the literature.[23]

Surface area and pore analysis

The porosity and pore volume distribution of the developed nano Fe-CNB observed in FE-SEM (Fig. 3C) is further explored by performing the BET surface area as shown in Fig. 4. The BET surface area is found to be 184.16 $m^2 g^{-1}$ with a pore diameter around 3.19 nm indicating the mesoporous nature of the material. The hysteresis loop of adsorption and desorption curve signifies Type IV indicating mono and multilayer adsorption on the surface exhibiting complete pore filling and capillary condensation.[5]

Thermal and magnetic behavior

To understand the thermal stability of the newly developed nano Fe-CNB TGA is performed for biopolymer sodium alginate and the nano Fe-CNB as shown in (Fig. S1, ESI†). The TGA for

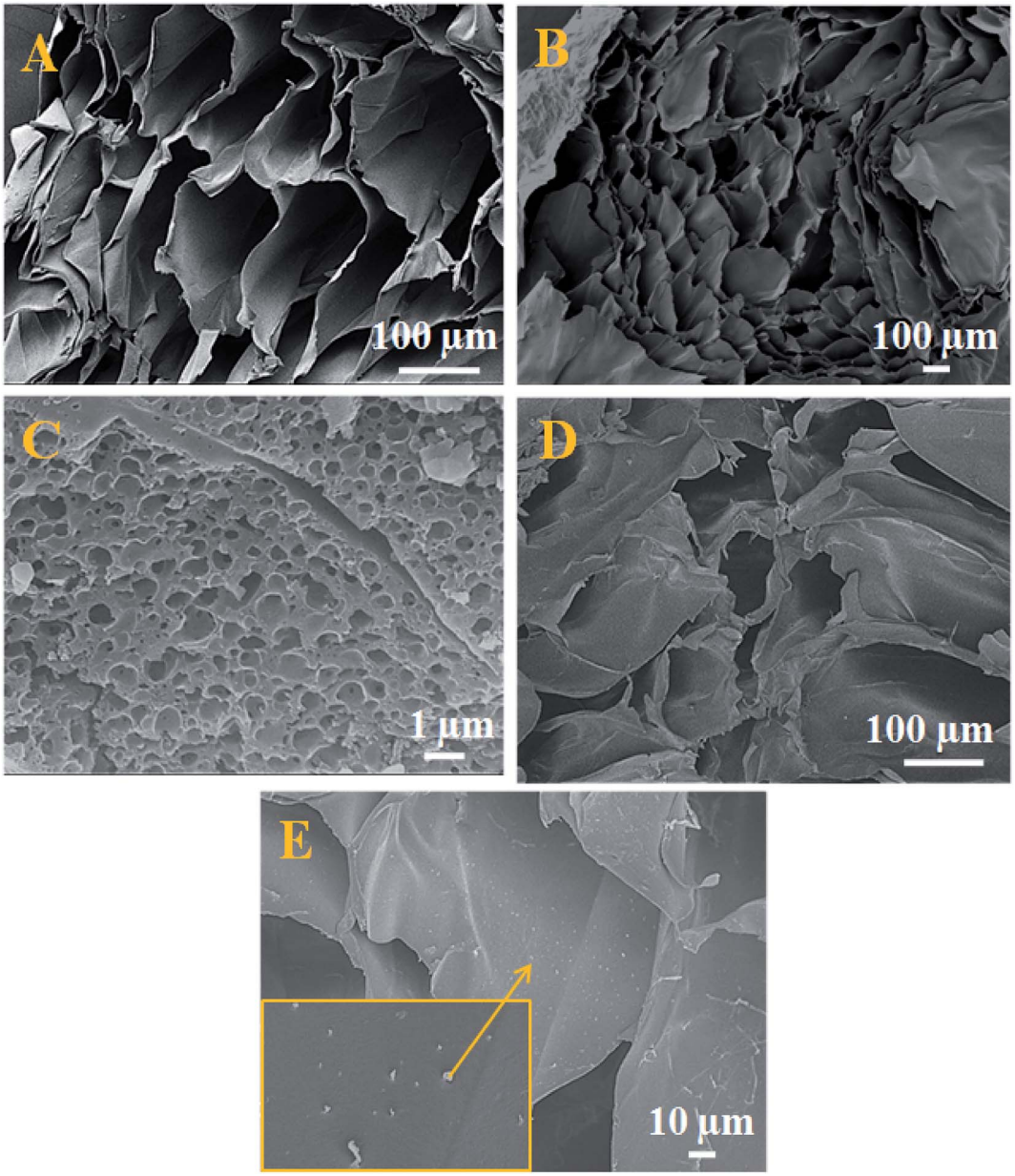

Fig. 3 FE-SEM for (A) cross-sectional view of CA beads indicate flake-like structure, (B) cross-sectional view after cutting the CA bead resembles the blooming of the flower bud. (C) Surface morphology for nano Fe-CNB porous nature, (D) cross-sectional view of nano-Fe CNB embedded CA beads exhibiting a layered material on its surface, (E) DOX-loaded on Fe-CNB CA beads cross-sectioned demonstrates the spherical particles present on the flakes.

sodium alginate exhibited two weight loss, initially the mass loss around 100 °C attributes to the removal of moisture present. The second mass loss is due to the break-down of polymeric chains around 250 °C. The TG for nano Fe-CNB exhibited initial moisture loss at 110 °C and the weight loss around 700 °C can be attributed due to the presence of Fe_3O_4.[24,25] The nano Fe-CNB is stable compared to the biopolymer. The amount of final residue at 800 °C for sodium alginate is 26.9% and 66.7% for nano Fe-CNB, which indicates the stability of nano Fe-CNB. This observation is consistent with literature for chitin based composite.[26]

The nano Fe-CNB used in this study exhibits magnetic behaviour in nature which is confirmed by the simple experiment of bringing a big magnet near the nano Fe-CNB powder. The experiment shows that under the influence of the magnetic field, the nano Fe-CNB particles are attracted to the big magnet. The image depicting the same is shown in (Fig. S2B, ESI†). In addition, the more detailed study to understand the magnetic property of nano Fe-CNB was performed using Vibrating Sample Magnetometer (VSM) as shown in (Fig. S2C, ESI†). The *M–H* curve exhibits negligible hysteresis indicating the superparamagnetism.[24,27] The high saturation magnetization (M_s) is observed at 11.2 emu g^{-1} (corresponding to 0.217 emu for 20 mg mass of the sample) which indicates the presence of magnetite (Fe_3O_4).[15,24,28]

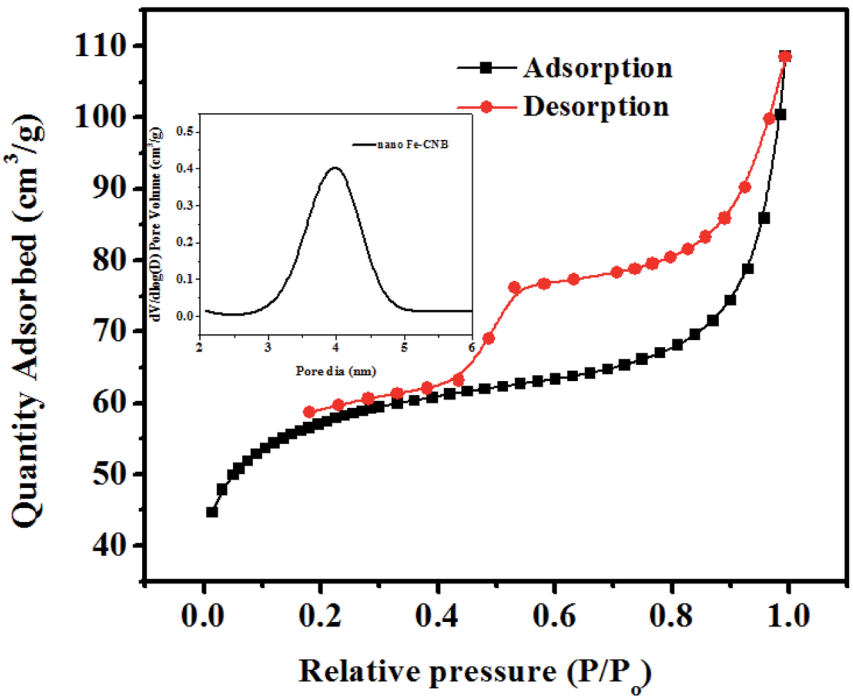

Fig. 4 BET analysis of nano-Fe-CNB: adsorption desorption hysteresis of nano-Fe-CNB indicating Type IV isotherm and pore volume distribution of nano-Fe-CNB indicating mesoporous nature of the material.

Spectroscopic analysis of the materials

Further, the confirmation of the presence of carbon material, Fe_3O_4, and α-Fe_2O_3 for nano Fe-CNB are obtained from Raman spectroscopy, as shown in Fig. 5. The Raman spectrum of carbon material generally consists of D, G, and 2D bands.[29,30] The D band is located near 1350 cm^{-1}, which indicates the presence of vacancies or dislocations in the graphene layer. The G band peak is located near 1580 cm^{-1}, which signifies the in-plane vibration of sp^2 hybridized carbon atoms. The ratio of the intensity of D band to G band (I_D/I_G) indicates the amount of defects present in the material.[31,32] The Raman spectrum for nano Fe-CNB is exhibited in Fig. 5, where the D band is observed at 1348 cm^{-1} and the G band at 1590 cm^{-1}, respectively which is in good agreement with those reported in the literature. The intensity ratio of D band to the G band (I_D/I_G) is observed to be 1.06, which indicates more defects in the carbon material. Thus, the defects in the material are attributed to the functionalization of graphitic carbon.[31] The spectrum around wavenumber 299 and 412 cm^{-1} correspond to α-Fe_2O_3,[33,34] and that of 668 cm^{-1} corresponds to Fe_3O_4.[24,35] However, the absence of a peak around wavenumber 721 cm^{-1} indicates that there is no maghemite.[24]

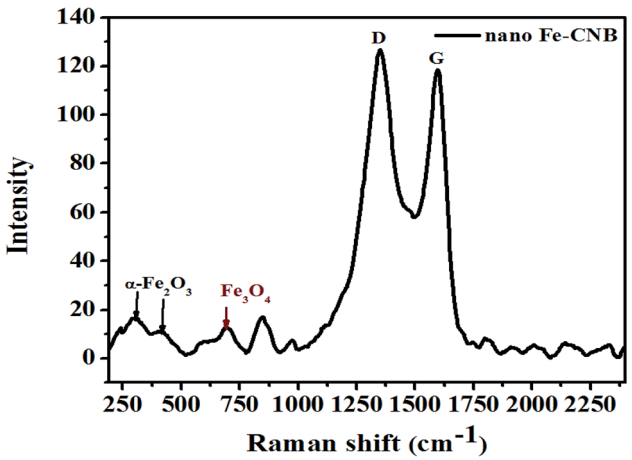

Fig. 5 Raman spectrum of nano-Fe-CNB to confirm the presence of carbon material, magnetite, and α-Fe_2O_3 corresponding to different wavenumbers. The ratio of the intensities of D and G band depicts the presence of defects in the carbon material.

The interaction studies for different materials are depicted with FTIR. While the chemical composition and the bond formation explicitly for the developed nano Fe-CNB is studied using XPS. Fig. 6A demonstrates the FTIR spectra of nano Fe-CNB material, calcium alginate, nano Fe-CNB loaded CA beads and DOX-loaded Fe-CNB CA beads. The nano-Fe-CNB (I) attributes the main characteristic peak for Fe_3O_4 around 630 cm^{-1} (ref. 13 and 21) (small hump exists but not quite visible due to the presence of very less quantity and scale used). Thus, the presence of Fe_3O_4 is in good agreement with the HR-TEM results (Fig. 2). Thus, Fe-CNB is a functionalized carbon-based layered material that is further confirmed by various analytical techniques. The characteristic peaks of alginate (II) were found at 3268, 1590, 1416, and 1029 cm^{-1} that corresponds to stretching of –OH, $–COO^-$ (asymmetric), $–COO^-$ (symmetric) and C–O–C respectively.[7,36] Also, nano Fe-CNB loaded CA beads (III) exhibits the characteristic peaks of alginate at 1029 cm^{-1} and 1590 cm^{-1}. When DOX is loaded on to nano Fe-CNB CA beads, the peak

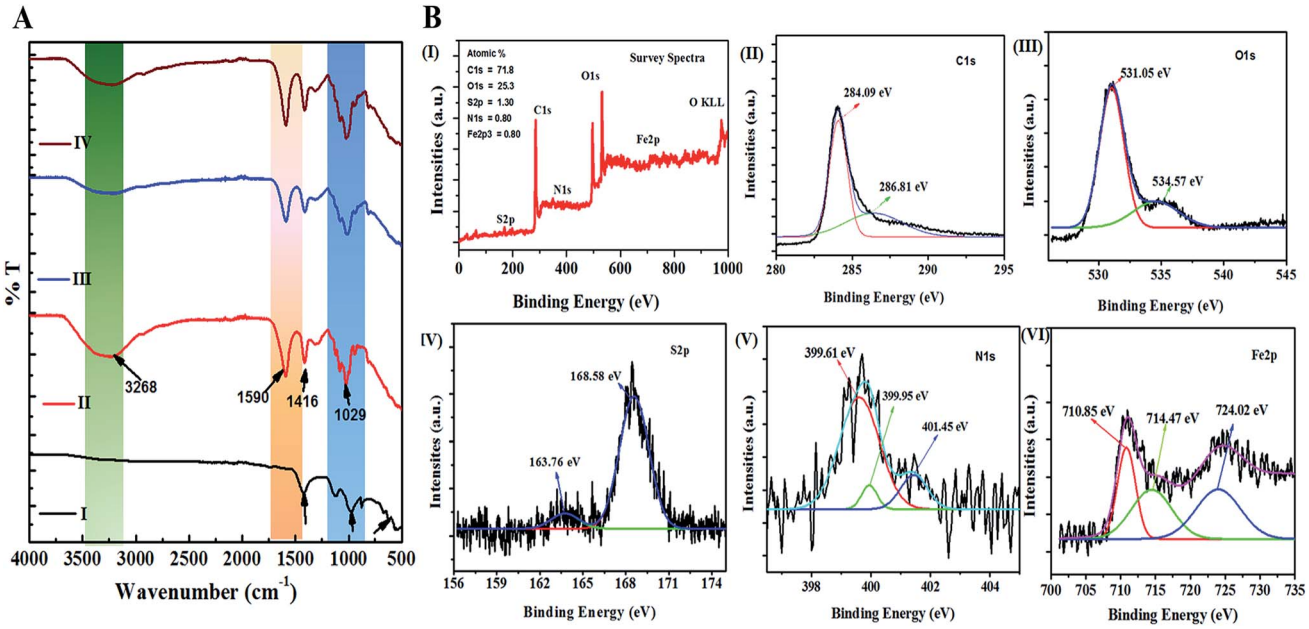

Fig. 6 (A) represents the FTIR for (I) nano Fe-CNB, (II) CA bead, (III) nano Fe-CNB embedded CA bead, (IV) DOX-loaded Fe-CNB CA bead to understand the presence of different functional groups and the interactions present in nano Fe-CNB, CA and DOX. (B) depicts the bond formation and chemical composition of nano Fe-CNB (I) survey spectra of nano Fe-CNB, (II) spectrum for C1s peak, (III) represents the O1s spectrum, (IV), (V) and (VI) represents the spectrum for S2p, N1s, and Fe2p of nano Fe-CNB respectively.

around 3298 cm^{-1} is observed at (IV). It may be attributed due to the presence of ($-NH_2$) groups of DOX.[37]

In addition, the XPS is performed for explaining the surface chemical composition and the information about the bonding, which is incorporated in Fig. 6B. The survey spectra confirm the presence of C1s, O1s, S2p, N1s, and Fe2p[3] corresponding to the peaks at binding energies 283 eV, 530 eV, 168 eV, 400 eV and 700 eV respectively[38,39] as shown in the Fig. 6B(I). The high-resolution XPS spectrum of C1s peak, shown in Fig. 6B(II), is deconvoluted into two components with binding energies 284.09 eV, 286.81 eV corresponding to the C–C/C=C and C–S/C–O/C–N respectively.[38,40] The O1s peak is deconvoluted into two components with binding energies 531.05 eV, and 534.57 eV, as shown in Fig. 6B(III) is attributed to the Fe–O and C–O–C.[28,41] Similarly, Fig. 6B(IV) represents the S2p, which is deconvoluted into two peaks centered at 163.76 and 168.58 eV, where the first peak is attributed to –C–S– covalent bond and other peak corresponds to the –C–SO_x– (x = 2, 3, 4) species.[42] The deconvoluted peak of N1s spectrum exhibited three peaks at 399.61 eV, 399.95 eV, 401.45 eV binding energy, as observed in Fig. 6B(V) corresponds to pyridinic, pyrrolic and graphitic nitrogen respectively.[38,43] The presence of the Fe_3O_4 in the nano Fe-CNB is confirmed due to the coexistence of Fe^{3+} and Fe^{2+} of Fe ($2p_{3/2}$) at binding energies 710.85 eV and 724.02 eV as observed in Fig. 6B(VI), whereas the presence of Fe_2O_3 is attributed to peak at binding energies 714.47 eV for Fe^{3+} oxidation state of Fe ($2p_{3/2}$).[38] Thus, XPS confirms the existence of C–C/C=C, C–S/C–O/C–N, Fe–O, C–O–C, –C–S–, –C–SO_x– and pyridinic, pyrrolic and graphitic nitrogen respectively in the nano Fe-CNB. These results are in good agreement with HR-TEM (Fig. 2) and Raman spectroscopy (Fig. 5).

Crystal properties

The crystalline nature and presence of different components in the nano bio-composite (nano Fe-CNB) are explored by P-XRD. Fig. 7 demonstrates the P-XRD data of nano Fe-CNB, calcium alginate, nano Fe-CNB embedded CA beads, and DOX-loaded Fe-CNB CA. Fig. 7A exhibits the magnified version of nano Fe-CNB with proper peak positions for different forms of iron. The presence of Fe in nano-composite is confirmed by the peaks at 2θ values 44.66° (110), 65.0° (200) and 82.31 (211) by PDF (03-065-4899). The 2θ values at 30.09° (220) and 35.44° (311) confirm the presence of Fe_3O_4, and the corresponding lattice planes are in agreement with PDF (01-086-1344). The α-Fe_2O_3 demonstrated 2θ values at 24.13° (012) and 63.94° (300) a match with PDF (00-033-0664). The graphitic carbon is evidenced by the presence of a peak at 2θ value 26.4°. The peaks at 2θ value 31.03° (004), 33.83° (112), and 42.95° (105) confirmed the presence of FeS, which is in good agreement with the PDF (01-089-6926). The presence of cohenite (Fe_3C) is confirmed by the appearance of a peak at 2θ value 52.0° (212) corresponding to PDF (00-035-0772). Thus, nano-Fe-CNB exhibits partially crystalline nature with the presence of Fe, Fe_3O_4, FeS, α-Fe_2O_3, cohenite, and graphitic carbon peak. The confirmation of the peak match is based on the ICDD database. The presence of Fe, Fe_3O_4, α-Fe_2O_3, and graphitic carbon is in agreement with the HR-TEM analysis (Fig. 2), Raman spectroscopy (Fig. 5), and XPS (Fig. 6) respectively.

Fig. 7B represents the diffraction of nano-Fe-CNB, which is elaborately explained in Fig. 7A. Calcium alginate is a naturally occurring amorphous bio-polymer. P-XRD represents the Halo peaks indicating the amorphous nature of calcium alginate.[44]

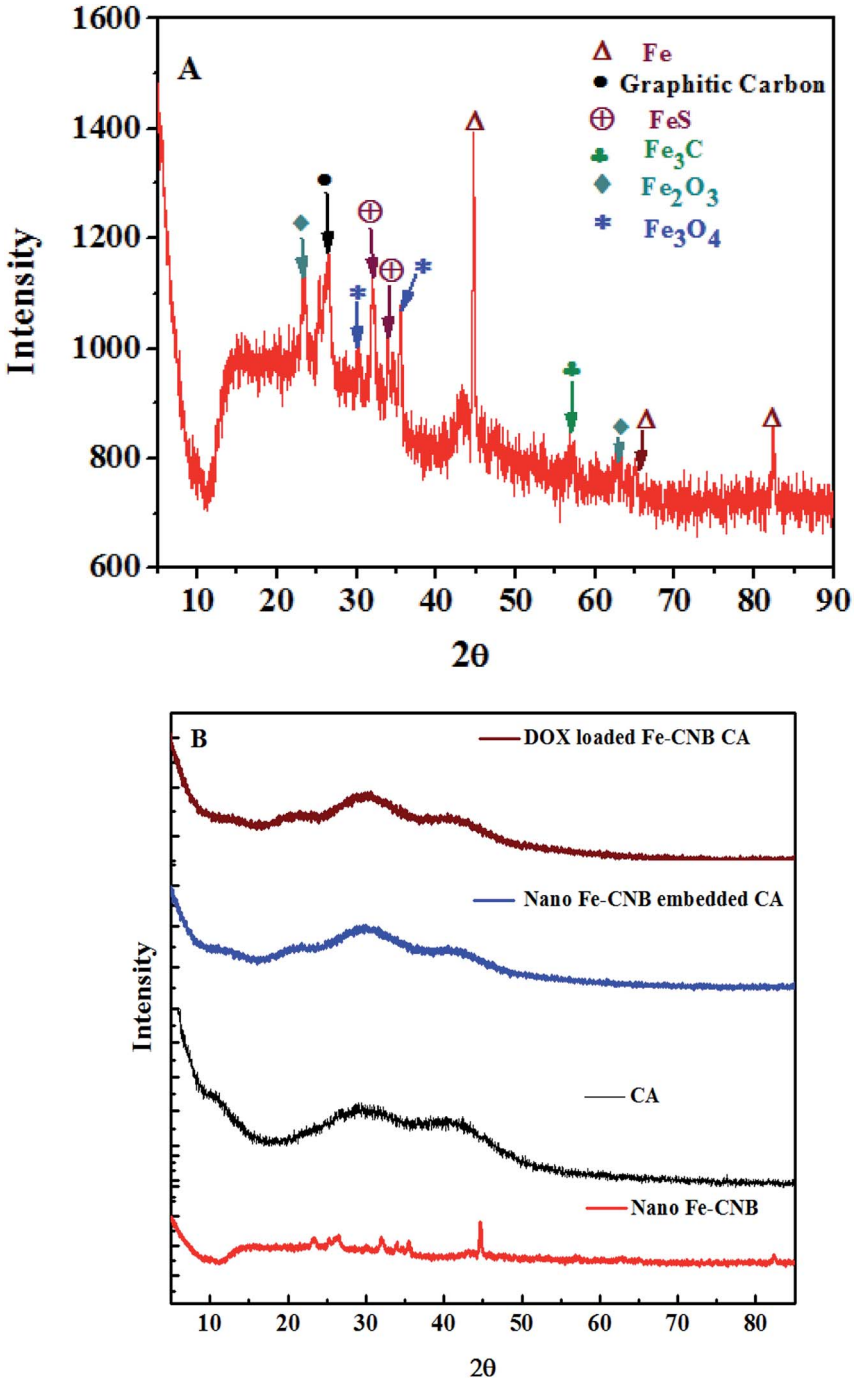

Fig. 7 P-XRD for (A) a magnified version of nano Fe-CNB to identify the different forms of iron present and the existence of graphitic carbon in the nano bio-composite, (B) P-XRD for nano Fe-CNB, calcium alginate bead, nano-Fe-CNB embedded CA beads and DOX-loaded nano-Fe-CNB embedded CA beads to determine the different forms of iron present in the nano-Fe-CNB and the crystalline nature of the material.

The addition of nano Fe-CNB (0.048 wt%) in amorphous calcium alginate also represents the halo peaks because of the dominating nature of the amorphous calcium alginate. DOX is a highly crystalline drug whereas, the diffraction of DOX-loaded Fe-CNB CA exhibits amorphous nature, indicating phase transformation of DOX from crystalline to amorphous form.[3,5]

Drug loading and release study

The DOX loading on control (CA) and nano Fe-CNB embedded CA is confirmed by the UV-vis spectrophotometer, as exhibited in Fig. 8A. The standard DOX solution (0.2 mg ml^{-1}) is prepared in Milli Q water at pH 7.4. The absorbance value of standard DOX solution is 0.993, while after 24 h the absorbance value decreases to 0.058 for nano-Fe-CNB embedded CA indicating 94.1 ± 0.1% drug loading by the nano Fe-CNB

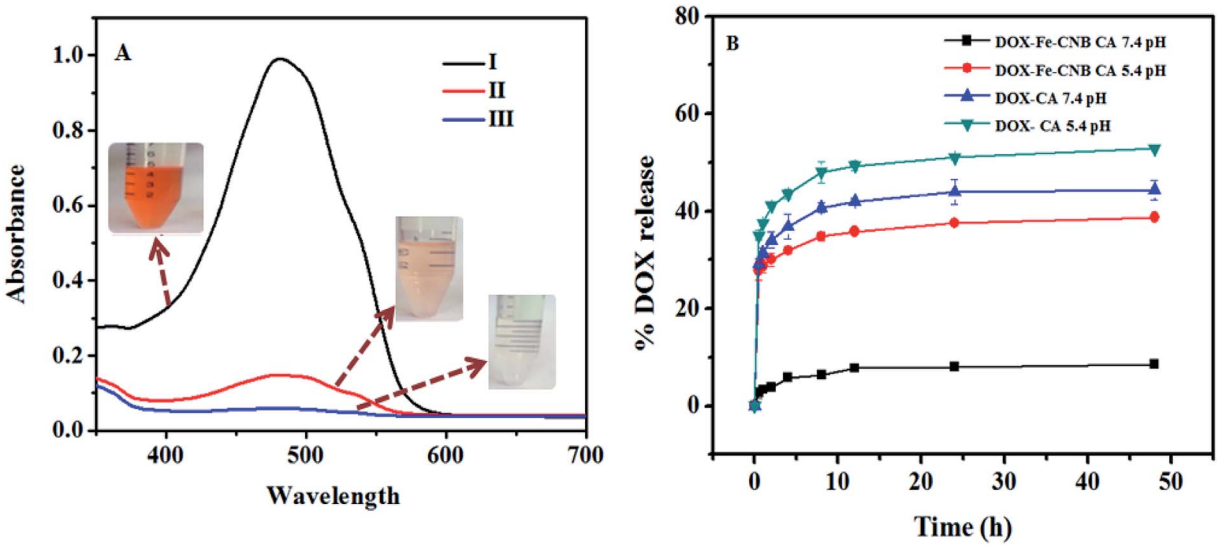

Fig. 8 (A) depicts the drug loading by UV absorption peak at ($\lambda = 480$ nm), (I) standard DOX solution, (II) decanted solution of the drug after DOX uptake by CA, (III) decanted solution of drug after DOX uptake by Fe-CNB CA. The reduced peak intensity demonstrates DOX loading in CA and Fe-CNB CA matrix. (B) represents the release of DOX-CA, and DOX-Fe-CNB CA at 5.4 and 7.4 pH. DOX-CA does not exhibit pH responsive behavior, while DOX-Fe-CNB CA depicts the pH responsive nature due to the addition of nano Fe-CNB and the controlled release of DOX is achieved at the end of 2 days.

embedded CA beads. Thus, the prepared nano Fe-CNB exhibited the improved loading efficiency of DOX. While the drug loading for CA bead without the addition of nano Fe-CNB is observed to be 78.3 ± 2.8%. The maximum uptake of DOX from standard solution is also evidenced visually by the disappearance of the color (DOX solution), as shown in Fig. 8A. Drug loading occurs mainly due to electrostatic interactions between anionic chains of alginate and cationic DOX, hydrogen bonds,[2,6,15] and π–π interactions.[17] On the other hand, high drug loading can be attributed to the complete pore filling of the nano Fe-CNB as evidenced by the BET surface area (Fig. 4) the mesoporous nano Fe-CNB plays a crucial role in loading along with the interaction sites of the prepared nanocomposite (nano Fe-CNB) material.

Possible drug loading mechanism on Fe-CNB CA

The possible interactions inside a hydrogel bead of DOX-loaded nano Fe-CNB CA are evidenced in the (Fig. S3, ESI†). Alginate is an anionic polymer which undergoes electrostatic interactions with cation Ca^{2+} ion of the $CaCl_2$ solution, and hydrogel bead is formed due to the egg-box model. The drug (DOX) is loaded onto nano-Fe-CNB embedded CA beads are due to following interactions. DOX being cationic drug and alginate being anionic, there exist strong electrostatic interactions between them, which facilitates drug loading. The π–π interactions take place between the DOX and the layered graphitic carbon material. The hydrogen-bond formation takes place among COO^- group of the polymeric alginate chain and OH^- a group of DOX (Fig. S3, ESI†). A sheet-like material represents the layered graphitic carbon sheet, which is embedded with the magnetic core (as evidenced through P-XRD (Fig. 7A) and HRTEM (Fig. 2F)). Thus, the MNP has good bio-compatible and magnetic responsive behavior and also enhance loading.[4,14] The MNP is hosted on the layered materials such as graphene, graphite, and CNT for their enhanced drug loading and pH-responsive behavior facilitating the controlled release.[4,14] These prevailing interactions may be responsible for the higher loading of DOX onto Fe-CNB CA beads.

Drug release behavior and statistical analysis

Fig. 8B represents the release of DOX from DOX-CA beads and DOX loaded-Fe-CNB CA beads at 5.4 and 7.4 pH, respectively. The rapid DOX release from DOX-loaded calcium alginate beads (control) is observed approximately up to 40.71% and 32.85% at 5.4 and 7.4 pH respectively at the initial 2 h. The release amount is further increased to 52.85% and 42.85% at 5.4 and 7.4 pH, respectively at the end of the 12 h. In contrast, the release of DOX from nano-Fe-CNB embedded CA beads at pH 5.4 and 7.4 pH is observed to be 29.03% and 3.87% at 5.4 and 7.4 pH at the initial 2 h. The release profile indicates that there is a gradual and sustained release of DOX at physiological pH is desirable. At the end of 2 days (48 h), only 8.3% of DOX is released at 7.4 pH. However, the DOX release at 5.4 pH is increased to 38.7%. This indicates the controlled release and pH responsive behavior of the Fe-CNB embedded CA beads. The DOX-loaded CA bead without the addition of nano Fe-CNB does not exhibit the pH response behavior, as observed by DOX-loaded Fe-CNB CA beads. These results signify the importance of the developed Fe-CNB CA for the controlled release of DOX. To compare the release of DOX from DOX-CA, and DOX-Fe-CNB CA at different pH that is 5.4 and 7.4 the statistical analysis is carried out using two way ANOVA (Graph Pad Prism version 5.0). The significance obtained is *** ($p < 0.001$) for $n = 3$ with SD.

Drug release mechanism

The more amount of drug is released at lower pH (acidic) is due to the protonation (H^+) of the amine group present in DOX.[2,3] The protonation loosens up the electrostatic interactions between cationic DOX and anionic polymeric chains and easily releases the DOX from the beads.[2] At alkaline pH, there is unprotonation, and strong electrostatic interactions prevail due to the presence of negative charges which arrest the DOX within the polymeric beads and thereby prevent the faster release of DOX.[2]

For further confirmation, the surface charge of the nano Fe-CNB layered material is performed by zeta potential measurements. The surface charge observed for nano Fe-CNB is -21.6 ± 3.84 at 5.4 pH and -28.6 ± 3.37 at 7.4 pH (physiological). However, the charge of the nano Fe-CNB is observed to move towards a positive charge from alkaline pH to acidic pH, indicating pH responsive behavior. The higher value of zeta potential measurements demonstrates the better stability irrespective of the surface charge (negative or positive). The higher drug loading percent on to nano Fe-CNB embedded CA beads (shown in Fig. 8) is due to not only its mesoporous nature but also due to the negative charge of nano Fe-CNB at pH 7.4 at which drug loading is carried out because DOX is a cationic drug. Thus, at physiological pH (7.4), not much DOX release is observed. However, release at tumor cells pH (5.4) is considerably high. Thus, the DOX release from DOX-loaded Fe-CNB CA exhibits pH responsive behavior and also ensures the therapeutic drug concentration at tumor cells. The studies are further extended to HeLa cell lines to understand the uptake of DOX from the DOX-loaded Fe-CNB CA and free DOX at different time intervals as shown (Fig. S4, ESI†). The fluorescence signal appears to be stronger for cells treated with free DOX as compared to that of DOX-loaded Fe-CNB CA for 24 h. The fluorescence signal of DOX-loaded Fe-CNB CA increases over a period of time, indicating the gradual and controlled release of DOX from DOX-loaded Fe-CNB CA. Thus, the developed iron based nano-biocomposite has the potential to reduce the undesirable side-effects associated with the burst release drugs.

Hence, the newly developed magnetic nano-biocomposite (nano Fe-CNB) prepared using seaweed biopolymer by one-step dry calcination is explored in detail using different characterization techniques. The FE-SEM and BET surface area depicts the morphology and pore nature of the newly developed nano Fe-CNB. The nano Fe-CNB is found to be mesoporous in nature having a surface area of 184.16 $m^2\ g^{-1}$ and a pore diameter around 3.19 nm. The size and the morphology of the nano-composite are explored in detail through the HR-TEM which exhibits the presence of 2-D layered graphitic material of thickness 7–8 nm decorated with Fe-based core (5–10 nm). The presence of graphitic carbon and different forms of iron (Fe_3O_4 and α-Fe_2O_3) is confirmed through P-XRD. These results are further examined by the Raman spectra which indicate the defects on the carbon material. Thus, all the characterization techniques revealed that the newly developed nano-biocomposite consists of 2-D layered graphitic carbon with different Fe-based core embedded on it.

The improved drug loading ~94% is attributed to the presence of 2-D layered graphitic carbon material in nano Fe-CNB which facilitates higher drug loading. This is due to the porous nature, high surface area, and hydrophobic interactions observed from FE-SEM, BET, HR-TEM, and Raman. The spectroscopic analysis such as FTIR and XPS demonstrate the presence of different hydroxyl and carboxyl groups which help to bind the drugs. The DOX exhibits the controlled release ~38% and ~8% release at pH 5.4 and 7.4 respectively. This implicates due to pH and magnetic responsive behavior of nano Fe-CNB evidenced by zeta and VSM measurements. The minimal release at physiological pH attributes to the strong electrostatic interactions prevailing between cationic DOX and the nano Fe-CNB which restricts the release of DOX at physiological pH and thereby reduces the side effects associated with it. However, at acidic pH the interactions reduce and the protonation of DOX facilitates more drug release at 5.4 pH. In addition, the magnetic studies of the nano Fe-CNB revealed that the saturation magnetization (M_s) exhibits negligible hysteresis indicating the material has the potential to be used in magnetic-based drug delivery systems.

Conclusions

In this study, we have developed a nano bio-composite (nano Fe-CNB) using alginate in combination with iron precursor by the dry process (calcination) without using any solvent, which is further embedded into alginate matrix for pH responsive drug carrier system. The developed nano Fe-CNB consist of graphitic layered material of thickness 7–8 nm with magnetic cores (d spacing 0.25 nm and size 5–10 nm). The developed nano Fe-CNB exhibits porous nature with surface area 184.16 $m^2\ g^{-1}$ with pore diameter of 3.19 nm. Raman spectroscopy of nano Fe-CNB further helped us to confirm the presence of Fe_3O_4, α-Fe_2O_3, and graphitic carbon. The XPS analysis of nano Fe-CNB indicates the existence of Fe–O, C–S, C–O, C–N, C–C/C=C. The developed nano Fe-CNB is thermally stable at high temperature confirmed by TGA, and magnetic behavior is evidenced by M–H hysteresis indicating supermagnetism. The P-XRD results of nano Fe-CNB further re-establishes the presence of graphitic carbon, Fe, Fe_3O_4, α-Fe_2O_3, FeS, Fe_3C. The magnetic nano Fe-CNB facilitates the higher doxorubicin loading (~94.1%) due to increased interactions with drug molecule. The release study shows that low release (8.3%) at physiological pH (7.4) and comparatively higher release (38.7%) at cancer cell pH (5.4) indicating the controlled release and the therapeutic drug concentration at tumor cell. At pH 7.4, nano Fe-CNB exhibits negative charge which facilitates the strong electrostatic interactions with cationic DOX and hence minimal release from the matrix. While at 5.4 pH the protonation of DOX takes place which weakens the electrostatic interactions between the matrix and easily releases DOX from the matrix. The developed magnetic nano Fe-CNB shows pH responsive behavior. Thus, newly developed magnetic nanoparticle embedded biopolymeric matrix can be considered as a potential smart drug delivery system for control release of anticancer drugs.

Conflicts of interest

Authors declare no competing interest.

Acknowledgements

Authors are thankful to IIT Gandhinagar for funding this work. SV express heartfelt gratitude to Nakshi Desai and Dr Bhaskar Datta for extending their help in cell culture experiments. SV and ND would also like to express gratitude to DSIR-IITGN Common Research & Technology Development Hub (CRTDH) instrumentation facilities and cell culture facilities of IITGN. Authors are thankful to IIT Kanpur for helping us with HR-TEM, Raman, and XPS facilities.

References

1 J. Ferlay, I. Soerjomataram, R. Dikshit, S. Eser, C. Mathers, M. Rebelo, D. M. Parkin, D. Forman and F. Bray, *Int. J. Cancer*, 2015, **136**, E359–E386.
2 S. Suarasan, M. Focsan, M. Potara, O. Soritau, A. Florea, D. Maniu and S. Astilean, *ACS Appl. Mater. Interfaces*, 2016, **8**, 22900–22913.
3 B. Manocha and A. Margaritis, *J. Nanomater.*, 2010, **2010**, 12.
4 L. Deng, Q. Li, S. a. Al-Rehili, H. Omar, A. Almalik, A. Alshamsan, J. Zhang and N. M. Khashab, *ACS Appl. Mater. Interfaces*, 2016, **8**, 6859–6868.
5 D. Kalaria, G. Sharma, V. Beniwal and M. R. Kumar, *Pharm. Res.*, 2009, **26**, 492–501.
6 Y. Xue, X. Xia, B. Yu, X. Luo, N. Cai, S. Long and F. Yu, *RSC Adv.*, 2015, **5**, 73416–73423.
7 S. Majumdar, G. Krishnatreya, N. Gogoi, D. Thakur and D. Chowdhury, *ACS Appl. Mater. Interfaces*, 2016, **8**, 34179–34184.
8 A. Nokhodchi, S. Raja, P. Patel and K. Asare-Addo, *BioImpacts*, 2012, **2**, 175.
9 K. Y. Lee and D. J. Mooney, *Prog. Polym. Sci.*, 2012, **37**, 106–126.
10 Y. Gao, Y. Chen, X. Ji, X. He, Q. Yin, Z. Zhang, J. Shi and Y. Li, *ACS Nano*, 2011, **5**, 9788–9798.
11 S. Pandey, M. Thakur, A. Mewada, D. Anjarlekar, N. Mishra and M. Sharon, *J. Mater. Chem. B*, 2013, **1**, 4972–4982.
12 R. Arvizo, R. Bhattacharya and P. Mukherjee, *Expert Opin. Drug Delivery*, 2010, **7**, 753–763.
13 A. H. Rezayan, M. Mousavi, S. Kheirjou, G. Amoabediny, M. S. Ardestani and J. Mohammadnejad, *J. Magn. Magn. Mater.*, 2016, **420**, 210–217.
14 J. Huang, Y. Li, A. Orza, Q. Lu, P. Guo, L. Wang, L. Yang and H. Mao, *Adv. Funct. Mater.*, 2016, **26**, 3818–3836.
15 J. Zeng, P. Du, L. Liu, J. Li, K. Tian, X. Jia, X. Zhao and P. Liu, *Mol. Pharmaceutics*, 2015, **12**, 4188–4199.
16 G. Prabha and V. Raj, *Mater. Sci. Eng. C*, 2017, **79**, 410–422.
17 X. Cao, L. Tao, S. Wen, W. Hou and X. Shi, *Carbohydr. Res.*, 2015, **405**, 70–77.
18 X. Zhang, L. Meng, Q. Lu, Z. Fei and P. J. Dyson, *Biomaterials*, 2009, **30**, 6041–6047.
19 Z. Ji, G. Lin, Q. Lu, L. Meng, X. Shen, L. Dong, C. Fu and X. Zhang, *J. Colloid Interface Sci.*, 2012, **365**, 143–149.
20 T. Zhou, X. Zhou and D. Xing, *Biomaterials*, 2014, **35**, 4185–4194.
21 V. Silva, P. Andrade, M. Silva, L. D. L. S. Valladares and J. A. Aguiar, *J. Magn. Magn. Mater.*, 2013, **343**, 138–143.
22 H. Khan, J. P. Chaudhary and R. Meena, *Int. J. Biol. Macromol.*, 2019, **124**, 1220–1229.
23 S. Patil, S. Gawali, S. Patil and S. Basu, *J. Mater. Chem. B*, 2013, **1**, 5742–5750.
24 S.-H. Hu, T.-Y. Liu, D.-M. Liu and S.-Y. Chen, *J. Controlled Release*, 2007, **121**, 181–189.
25 E. T. Tenório-Neto, T. Jamshaid, M. Eissa, M. H. Kunita, N. Zine, G. Agusti, H. Fessi, A. E. El-Salhi and A. Elaissari, *Polym. Adv. Technol.*, 2015, **26**, 1199–1208.
26 M. Ramesan, P. Privya, P. Jayakrishnan, G. Kalaprasad, B. Bahuleyan and M. Al-Maghrabi, *Polym. Compos.*, 2018, **39**, E540–E549.
27 Z. Lu, Y. Xu and S. Zhou, *RSC Adv.*, 2017, **7**, 42363–42369.
28 E. Bian, Y. Xu, S. Lou, Y. Fu and S. Zhou, *J. Nanopart. Res.*, 2016, **18**, 331.
29 A. Maulana, A. Nugraheni, D. Jayanti, S. Mustofa and M. Baqiya, *IOP Conf. Ser.: Mater. Sci. Eng.*, 2017, **196**(1), 012021.
30 A. C. Ferrari, *Solid State Commun.*, 2007, **143**, 47–57.
31 R. Muzyka, S. Drewniak, T. Pustelny, M. Chrubasik and G. Gryglewicz, *Materials*, 2018, **11**, 1050.
32 G. Calderon-Ayala, M. Cortez-Valadez, P. Mani-Gonzalez, R. B. Hurtado, J. Contreras-Rascón, R. Carrillo-Torres, M. E. Zayas, S. Castillo, A. Hernández-Martínez and M. Flores-Acosta, *Carbon Lett.*, 2017, **21**, 93–97.
33 J.-f. Lu and C.-J. Tsai, *Nanoscale Res. Lett.*, 2014, **9**, 230.
34 G. Bharath and N. Ponpandian, *RSC Adv.*, 2015, **5**, 84685–84693.
35 S. Majumder, S. Dey, K. Bagani, S. Dey, S. Banerjee and S. Kumar, *Dalton Trans.*, 2015, **44**, 7190–7202.
36 N. Gogoi and D. Chowdhury, *J. Mater. Chem. B*, 2014, **2**, 4089–4099.
37 S. P. Victor, W. Paul, M. Jayabalan and C. P. Sharma, *CrystEngComm*, 2014, **16**, 9033–9042.
38 A. Ghosh, S. Ghosh, G. M. Seshadhri and S. Ramaprabhu, *Sci. Rep.*, 2019, **9**, 5187.
39 J. P. Chaudhary, R. Gupta, A. Mahto, N. Vadodariya, K. Dharmalingm, N. Sanna Kotrappanavar and R. Meena, *ACS Sustainable Chem. Eng.*, 2018, **7**, 174–186.
40 Y. Dong, H. Pang, H. B. Yang, C. Guo, J. Shao, Y. Chi, C. M. Li and T. Yu, *Angew. Chem., Int. Ed.*, 2013, **52**, 7800–7804.
41 Z. Yang, M. Xu, Y. Liu, F. He, F. Gao, Y. Su, H. Wei and Y. Zhang, *Nanoscale*, 2014, **6**, 1890–1895.
42 D. Sun, R. Ban, P.-H. Zhang, G.-H. Wu, J.-R. Zhang and J.-J. Zhu, *Carbon*, 2013, **64**, 424–434.
43 Z.-L. Wang, D. Xu, H.-X. Zhong, J. Wang, F.-L. Meng and X.-B. Zhang, *Sci. Adv.*, 2015, **1**, e1400035.
44 K. M. Rao, K. K. Rao, P. Sudhakar, K. C. Rao and M. C. S. Subha, *J. Appl. Pharm. Sci.*, 2013, **3**(6), 61–69.

